

Supplementary Information

Experimental and theoretical investigations of the effect of heteroatom doped Carbon microsphere support on stability and storage capacity of nano- Co_3O_4 conversion anode for Lithium-ion batteries

Pravin K. Dwivedi^{ab}, Aathira Nair^a, Rupali S. Mehare^{ab}, Vikash Chaturvedi^{ab}, Kavita Joshi^{ab*} and Manjusha V. Shelke^{ab*}

^a Physical and Materials Chemistry Division, CSIR-National Chemical Laboratory, Pune 411008, MH, India.

^b Academy of Scientific and Innovative Research (AcSIR), Gaziabad 201002, UP, India.

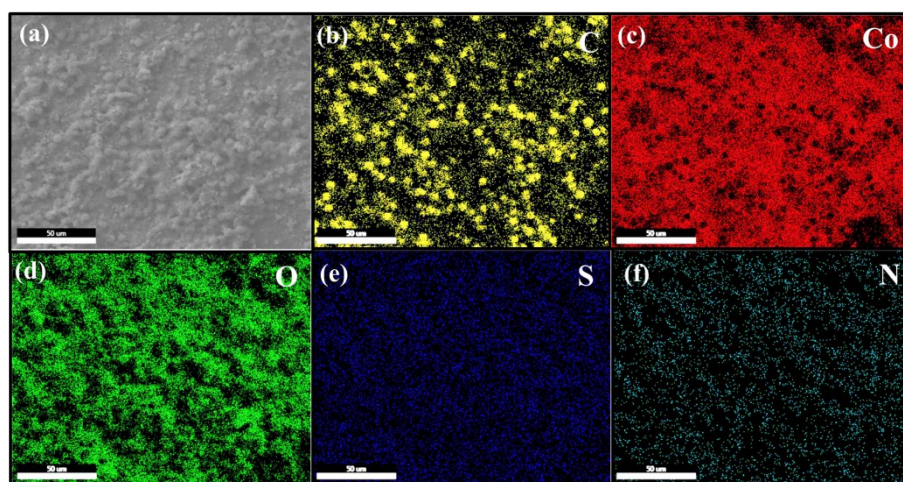


Figure S1. (a) ESEM elemental mapping images of (b) C, (c) Co, (d) O, (e) S and (f) N.

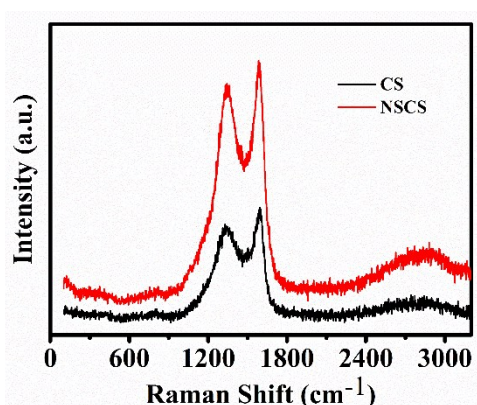


Figure S2. (a) The Raman spectra of CS and NSCS.

Raman spectrum was carried out to further investigate the graphitic and disordered nature of the Carbon sphere and N and S Doped carbon sphere (Figure S2). The Raman spectra of CS and NSCS contain peaks centered near 1350 cm^{-1} and 1592 cm^{-1} , which are the D and G bands respectively, as shown in figure S2. The D band arises from the vibrations of carbon atoms with dangling bonds in plane terminations, and is thus related to the defects of graphitic carbon, whereas the G band arises from the vibrations of sp^2 carbon atoms in the graphitic layer. The ratio of the integrated areas of the D and G bands (ID/IG) of CS and NSCS were estimated using Gaussian curve fit and found 2.6 and 2.8, respectively. [1, 2]

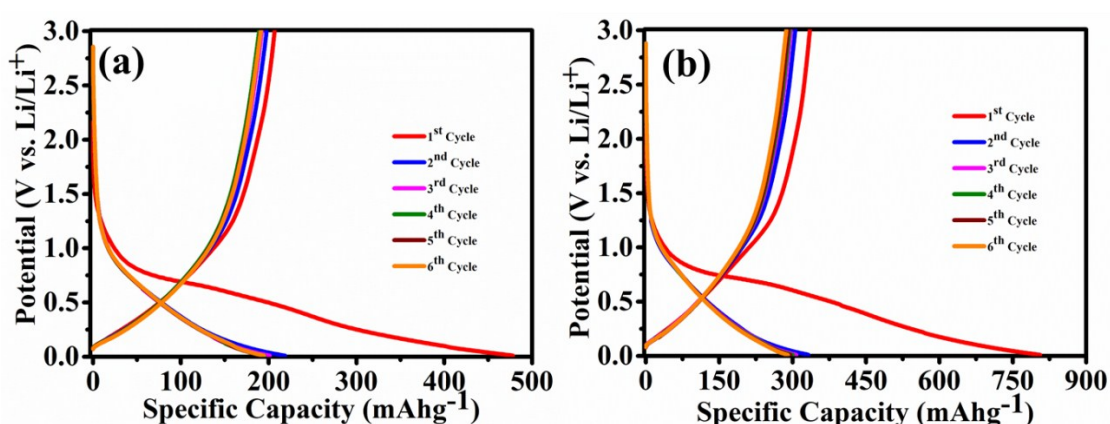


Figure S3: Galvanostatic charge-discharge profiles of (a) CS (b) NSCS electrode at current density of 100 mA g^{-1} .

The galvanostatic charge-discharge profiles of the CS and NSCS for first six cycles at a current density of 100 mA g^{-1} between 0.01-3 V are presented in the figure S3a and S3b. Specific discharge capacities for CS and NSCS are found to be around 251 and 317 mAhg^{-1} respectively at second cycle. Higher specific discharge capacity of NSCS is due to the hetero atoms (N and S) in the carbon matrix. The large initial capacity loss in both the samples can be attributed to the irreversible storage of Li-ions in to the carbon matrix and electrolyte decomposition resulting in to the formation of SEI film.

Figure S4a shows the Nyquist plots for NSCS- Co_3O_4 electrode in a fresh cell and after 10^{th} , 30^{th} , 60^{th} , 250^{th} cycles of charge-discharge at 1 Ag^{-1} of current density. It can be seen in the impedance spectrum that the charge transfer resistance of the cell decreases after 10^{th} cycle, whereas charge transfer resistance and Warburg impedance both increased after 30^{th} and 60^{th} cycles. This could be probably due to structural changes occurring in the electrode material for a few cycles after the activation process. The impedance spectrum taken after 250 cycles shows two prominent semicircles, one at the higher frequency range corresponding to the SEI layer resistance and the one at mid frequency corresponding to charge transfer resistance. It is observed that after 250 cycles, both the Warburg as well as charge transfer resistance of the cell decreased on account of SEI layer formation with

optimum thickness on the electrode surface and enhanced electronic/ionic transport due to electrolyte penetration leading to the increased specific capacity of the electrode. [3, 4] Thus, the impedance measurement of the cell at different levels of cycling validates the cycle life study.

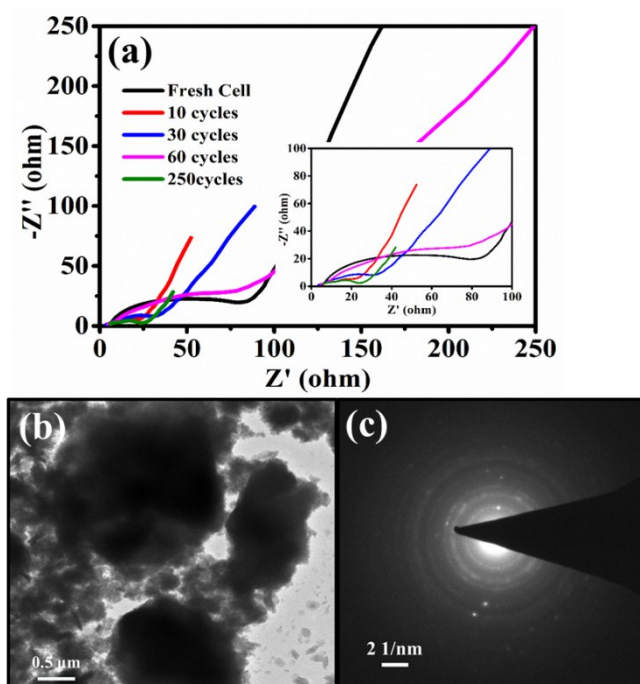


Figure S4: (a) Impedance spectra of NSCS-Co₃O₄ nanocomposite at different cycle number during cycling at 1 Ag⁻¹ (b) TEM images and (c) SAED pattern of NSCS-Co₃O₄ nanocomposite electrode after 350 cycles at 1 Ag⁻¹.

Furthermore, figure S4b represents the TEM images of the NSCS-Co₃O₄ electrode cycled at 1 Ag⁻¹ over 350 cycles. It can be seen that the morphology of the NSCS-Co₃O₄ nanocomposites is still retained after a large number of charge-discharge cycles. A SAED pattern of the same electrode after the 350 cycles is presented in figure S4c; from the observations, it appears that the electrode material has partially retained its polycrystalline nature after 350 charge-discharge cycles.

Table S1. Comparative study of electrochemical performance of Co₃O₄/Carbon composites as an anode for Li - ion battery.

Electrode Material	Cycling stability	Specific capacity (mAhg ⁻¹)	Reference
Co ₃ O ₄ /nitrogen doped graphene	1328 mAhg ⁻¹ at 0.1 A g ⁻¹ , 200 cycle	700 (1 Ag ⁻¹)	5
Sandwich-like Co ₃ O ₄ /Graphene	1113 mAhg ⁻¹ , at 0.2 A g ⁻¹ , 100 cycle	899.8 (1 Ag ⁻¹)	6

Graphene/Co ₃ O ₄ nanotubes	961.4 mAhg ⁻¹ , at 0.1 A g ⁻¹ , 80 cycle	~600 (0.8 Ag ⁻¹)	7
6Plasma-treated Co ₃ O ₄ /graphene	1269 mAhg ⁻¹ , at 0.125 Ag ⁻¹ , 50 cycle	400 (0.95 Ag ⁻¹)	8
Co ₃ O ₄ /CC@Graphene	391 mAhg ⁻¹ , at 0.1 Ag ⁻¹ , 300 cycle	473 (0.1 Ag ⁻¹)	9
Co ₃ O ₄ -graphene sheet-on-sheet	1065 mAhg ⁻¹ , at 0.1 Ag ⁻¹ , 30 cycle	1235 (0.1 C)	10
Co ₃ O ₄ /Graphene	1095 mAhg ⁻¹ , at 0.2 Ag ⁻¹ , 100 cycle	1480 (0.1 Ag ⁻¹)	11
Co ₃ O ₄ /porous carbon nanofibers	825.6 mAhg ⁻¹ at 0.1 C, 50 cycles	869.5 mAhg ⁻¹ (0.1 C)	12
Carbon-Encapsulated Co ₃ O ₄ Nanoparticles	760 mAhg ⁻¹ at 5 C, 1000 cycles	1413 mA h g ⁻¹ (0.1Ag ⁻¹)	13
Three-dimensional (3D) mesoporous Co ₃ O ₄ /CA	779 mAhg ⁻¹ at 50 mAg ⁻¹ , 50 cycles	987 mAhg ⁻¹ (50 mAg ⁻¹)	14
Co ₃ O ₄ /MWCNT hybrid nanostructures	940 mAg ⁻¹ at 0.2 C, 70 cycles	750 mAhg ⁻¹ (0.2 C)	15
Co3O4-NSCS	1285 mAhg⁻¹ at 1 Ag⁻¹, 350 cycles	1807 mAhg⁻¹ (0.1 Ag⁻¹)	This work

References:

1. K. Sun, Y. Hu, X. Zhang, K. San Hui, K. Zhang, G. Xu, J. Ma and W. He, *Electrochim. Acta*, 2020, **335**, 135680.
2. S. C. Ray, Z. N. Tetana, R. Erasmus, W.-F. Pong and N. J. Coville, *Appl. Phys. A*, 2014, **115**, 153-157.
3. Y. Bai, X. Wang, X. Zhang, H. Shu, X. Yang, B. Hu, Q. Wei, H. Wu and Y. Song, *Electrochim. Acta*, 2013, **109**, 355-364.
4. T. Liu, A. Garsuch, F. Chesneau and B. L. Lucht, *J. Power Sources*, 2014, **269**, 920-926.
5. X. Xing, R. Liu, S. Liu, S. Xiao, Y. Xu, C. Wang and D. Wu, *Electrochim. Acta*, 2016, **194**, 310-316.
6. Y. Yang, J. Huang, J. Zeng, J. Xiong and J. Zhao, *ACS Appl. Mater. Interfaces*, 2017, **9**, 32801-32811.
7. D. Li, Q. Lu, E. Guo, M. Wei, Z. Xiu and X. Ji, *J. Sol-Gel Sci. Technol.*, 2017, **82**, 75-84.
8. H. Long, M. Zhang, Q. Wang, L. Xing, S. Wang and X. Xue, *J. Alloys Compd.*, 2017, **701**, 200-207.
9. Q. Xie, Y. Zhang, Y. Zhu, W. Fu, X. Zhang, P. Zhao and S. Wu, *Electrochim. Acta*, 2017, **247**, 125-131.

10. Q. Su, W. Yuan, L. Yao, Y. Wu, J. Zhang and G. Du, *Mater. Res. Bull.*, 2015, **72**, 43-49.
11. S. Wang, R. Wang, J. Chang, N. Hu and C. Xu, *Sci. Rep.*, 2018, **8**, 3182.
12. H. Yang, Y. Wang, Y. Nie, S. Sun and T. Yang, *J. Compos. Mater.*, 2016, **51**, 315-322.
13. X. Leng, S. Wei, Z. Jiang, J. Lian, G. Wang and Q. Jiang, *Sci. Rep.*, 2015, **5**, 16629.
14. F. Hao, Z. Zhang and L. Yin, *ACS Appl. Mater. Interfaces*, 2013, **5**, 8337-8344.
15. Z. Fang, W. Xu, T. Huang, M. Li, W. Wang, Y. Liu, C. Mao, F. Meng, M. Wang, M. Cheng, A. Yu and X. Guo, *Mater. Res. Bull.*, 2013, **48**, 4419-4423.